

# Aggregation-induced and crystallization-enhanced emissions with time-dependence of a new Schiff-base family based on benzimidazole†

Cite this: *J. Mater. Chem. C*, 2014, 2, 3686

Yuanle Cao,<sup>a</sup> Mingdi Yang,<sup>\*ab</sup> Yang Wang,<sup>a</sup> HongPing Zhou,<sup>\*a</sup> Jun Zheng,<sup>c</sup> Xiuzhen Zhang,<sup>a</sup> Jieying Wu,<sup>a</sup> Yupeng Tian<sup>a</sup> and Zongquan Wu<sup>d</sup>

A new Schiff-base family containing [4-(1*H*-benzimidazole-2-yl)-phenyl]-bis-(4-ethoxy-phenyl)-amine has been synthesized through a condensation reaction. All the derivatives possess properties of aggregation-induced and crystallization-enhanced emission (AIE and CEE), which show time-dependent characteristics at a concentration of 10  $\mu\text{M}$  and are studied in detail by scanning electron microscope (SEM) and transmission electron microscope (TEM). Different aggregation forms and the growth of crystals of the compounds, could be responsible for the notably different degrees of fluorescence enhancement.

Received 3rd January 2014  
Accepted 10th February 2014

DOI: 10.1039/c3tc32551b

[www.rsc.org/MaterialsC](http://www.rsc.org/MaterialsC)

## Introduction

Organic fluorescent materials have attracted intensive interest because of their potential applications in organic light-emitting diodes (OLEDs), fluorescent sensors, *etc.*<sup>1</sup> However, many dyes emit strongly when dissolved in good solvents, but become weakly luminescent when fabricated into solid films or aggregated in poor solvents.<sup>2</sup> This phenomenon is notoriously known as aggregation-caused quenching (ACQ).

The ACQ effect has greatly limited the applications of organic luminescent materials and has driven researchers to seek anti-ACQ materials with higher efficiency in the aggregated state than in the dissolved state. Several anti-ACQ materials were reported by Tang *et al.*<sup>3</sup> and Park *et al.*<sup>4</sup> in 2001 and 2002, respectively, and these substances are termed aggregation-induced emission (AIE) and aggregation-induced enhancement emission (AIEE) materials. Some of these materials show a special phenomenon of AIE or AIEE in aqueous mixtures in the crystal state form, which has been designated as crystallization-enhanced emission (CEE).<sup>5</sup> Many crystalline AIE materials have been found to exhibit high fluorescence efficiencies compared to their amorphous counterparts. The AIE or CEE effect was

previously attributed to the restricted intramolecular rotation (RIR) mechanism. Although the mechanism of AIE or CEE has been studied for a period of time, the number of the AIE or CEE materials is quite limited, for example, silole-based compounds and arylethene derivatives.<sup>6</sup> To further enlarge the family of specific AIE-active compounds, it is necessary to carry out more extensive investigations in this field.

Recently, the synthesis and application of triphenylamine (TPA) derivatives as emissive materials have been of great interest for chemists and material scientists due to their charge-transport properties, and thermal stability.<sup>7</sup> TPA derivatives, however, usually give a strong emission in organic solvent, but suffer from the notorious effect of ACQ in the condensed phase. Benzimidazole, a conjugated compound with good bioactivity, is usually used as a medical intermediate.<sup>8</sup> The combination of two compounds may lead to the generation of a new system with enhanced conjugation and bioactivity. A small aromatic ring attached to benzimidazole by a single bond may activate the radiative transition channel to some extent, which could endow the compounds with AIE or AIEE properties.

We are interested in and have worked on the exploration of new AIE or CEE systems.<sup>9</sup> In this work, we synthesise six novel TPA-substituted benzimidazole-based conjugated Schiff bases. During the study, we discovered that the compounds emit fluorescence in the solvent mixtures with low water contents containing crystals, but become non-luminescent, even in the mixtures with a high water content containing homogeneous nano-particles, which can be attributed to the AIE or CEE process. The intramolecular motions of the compounds remain active in the amorphous phase and can be suppressed by crystal formation, thus causing the novel CEE effect. The AIE and CEE phenomena of the compounds are accompanied by time-dependent intensity enhancement. This behavior may be

<sup>a</sup>College of Chemistry and Chemical Engineering, Anhui University and Key Laboratory of Functional Inorganic Materials Chemistry of Anhui Province, Hefei 230601, P. R. China. E-mail: zhpzhp@263.net; Fax: +86-551-63861279; Tel: +86-551-63861279

<sup>b</sup>School of Materials and Chemical Engineering, Anhui Jianzhu University, Hefei 230601, P. R. China. Fax: +86-551-63828106; Tel: +86-551-63828150

<sup>c</sup>Center of Modern Experimental Technology, Anhui University, Hefei 230039, P. R. China

<sup>d</sup>School of Chemical Engineering, Hefei University of Technology, Hefei 230009, P. R. China

† Electronic supplementary information (ESI) available: Fig. S1–S10, Tables S1–S3. See DOI: 10.1039/c3tc32551b

induced by the constantly changing size and morphology of the nanoparticles under the impact of solvent, such as water.<sup>10</sup>

## Results and discussion

### Synthesis

The synthetic routes to compounds 1–6 and their intermediates are depicted in Scheme 1. The detailed procedures for the syntheses of the intermediates and final products are described in the experimental section. The targeted compounds 1–6 were obtained by the condensation of an aldehyde and amine.

### Absorption and photoluminescence properties

Fig. 1 and 2 show the absorption and fluorescence spectra of compounds 1 and 5 (the others are in Fig. S1 and S2†) in different polar solvents (dichloromethane (DCM), tetrahydrofuran (THF), ethanol, acetonitrile, *N,N*-dimethyl formamide (DMF) and dimethylsulfoxide (DMSO)).

As seen in Fig. 1 and Table S1,† the polarity of the solvents had little effect on the absorption wavelengths of compounds 1 and 5 (2–4, 6 in Fig. S1†), but exerted a great influence on the photoluminescence (PL) emission (1 and 5 in Fig. 2, 2–4, 6 in Fig. S2†). For example, the maximum absorption wavelength ( $\lambda_a$ ) of compound 1 is located at 373–381 nm, however, the maximum emission wavelength ( $\lambda_e$ ) varied from 437 nm to 470 nm. The  $\lambda_a$  and  $\lambda_e$  (Table S1†) of 1–3 in different solvents are almost the same, which reveals that the different location of the N in pyridine has no obvious effect on the maximum emission wavelengths of 1–3.

To better understand the photophysical properties of the compounds, we performed theoretical calculations with the

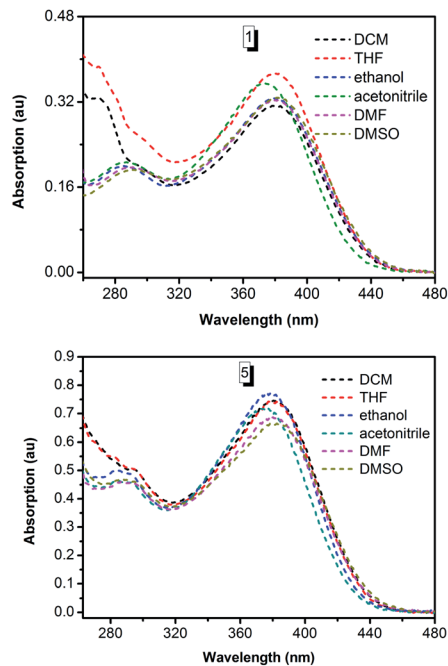
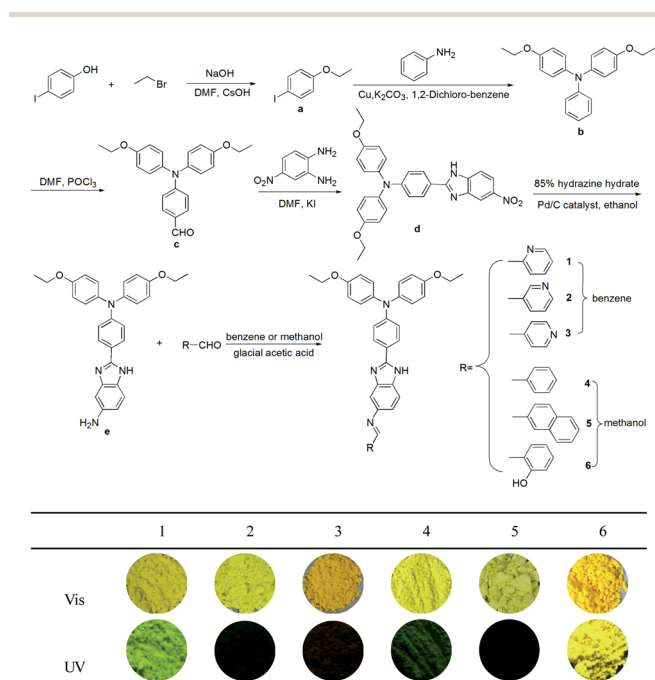


Fig. 1 Absorption spectra of compounds 1 and 5 in different polar solvents. Concentration of the solutions: 10  $\mu$ M.

density functional of B3LYP/6-31G(d). The optimized geometries and HOMO (Highest Occupied Molecular Orbital)/LUMO (Lowest Unoccupied Molecular Orbital) plots of 1–6 are illustrated in Fig. 3. All of the molecules adopt twisted non-planar conformations at the terminal aromatic ring, which is favorable for active intramolecular rotations of the aromatic ring in pure



Scheme 1 Synthetic routes to compounds 1–6 and photographs of their solids taken under visible and UV light.

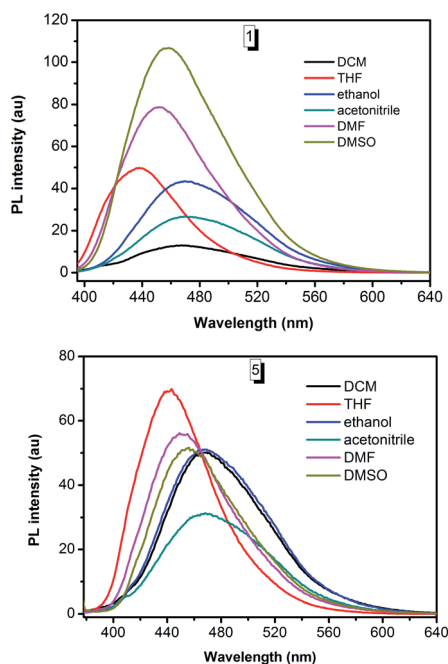


Fig. 2 Fluorescence spectra of compounds 1 and 5 in different polar solvents (10  $\mu$ M).

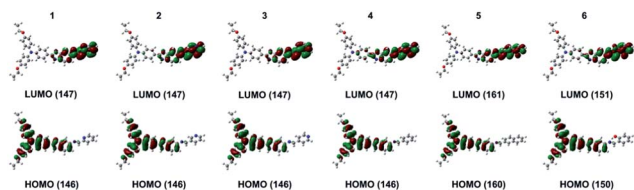


Fig. 3 Energy level and electron density distribution of the frontier orbitals of compounds 1–6.

solutions. In spite of the values of the band gap ( $\Delta E_g$ ) differing (Table S2<sup>†</sup>), the compounds have very similar maximum absorption and emission wavelengths in the same solvents, indicating the potential influence of molecular rotation on band gaps in the excited state.

Obviously, the electron clouds of the HOMOs and LUMOs of compounds 1–6 are dominated by the triphenylamine section and aromatic ring at the ends of the molecules, respectively, which means that their absorption and emission primarily stem from the ICT (intramolecular charge transfer) transitions. However, the emission behavior of compounds 1–6 in solvents as described above is strikingly different from that of conventional ICT systems, which are nonfluorescent in highly polar solvents, but intensely emissive in nonpolar solvents. Thus the formation of aggregation may restrain the ICT process in the solution mixture to some extent, which is helpful for the light emission.<sup>11</sup>

### AIE and CEE phenomena

The dilute THF solutions of 1–6 ( $1 \times 10^{-5}$  mol L<sup>-1</sup>) were transparent and displayed very faint lights with emission maximums peaking in the region of 450 nm when excited at 380 nm at room temperature (Table 1).

The absorption spectra of 1 and 5 in the THF–water mixtures are shown in Fig. 4. The spectrum profile was virtually unchanged when a low water fraction was injected into the THF solution. However, the absorption curves of 1–6 in the THF–water mixtures with a relatively high water fraction ( $\geq 60\%$ ) decayed further from zero, even in the long wavelength region, indicative of the existence of aggregative species in these solvent mixtures.<sup>12</sup> The maximum absorption wavelength of 1 undergoes a blue-shift from 381 nm (in pure THF solvent) to 361 nm (at 50% water fraction), and then a red-shift to 373 nm (at

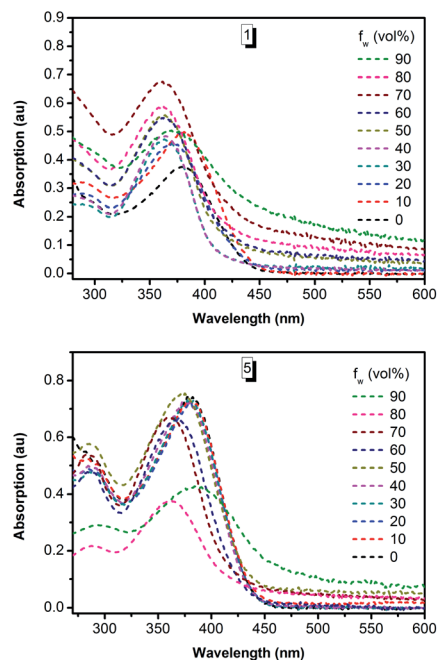


Fig. 4 UV absorption spectra of 1 and 5 in water–THF mixtures with different volume fractions of water after water was injected for 1 h (10  $\mu$ M).

90% water contents), indicating that during the self-assembly of the emitting species the states of aggregation may have changed. The same tendency can also be found in the absorption spectra of the other compounds (Fig. S3<sup>†</sup>).

The luminescence behavior of the water–THF mixtures with different water contents after water was injected for 24 hours is shown in Fig. 5 (2–4, 6 in Fig. S4<sup>†</sup>). In pure THF, the emissions of the compounds are very weak and virtually invisible. However, strong blue and cyan emission can be exhibited in the solvent mixtures with 30% and 60% water contents, respectively. The absorption and emission behaviors of 1 in the pure THF and THF–water mixtures may be understood as follows. In the isolated state, that is the molecule completely dissolved in good solvent, the active intramolecular rotations of the terminal aromatic ring effectively deactivated its excited species, hence the faint light emission can be observed. Since the formation of aggregation can rigidify the molecular conformation and thus block the nonradiative relaxation channel, the excited state decays radiatively. As a result, 1 becomes highly emissive in the aggregation state. As the proportion of water further increases to a certain degree (90%), no fluorescence can be observed again (insets in Fig. 5 and S4<sup>†</sup>). All of the compounds show an emission enhancement at a low water fraction, but a decrease at a high water fraction, which exhibits a down-top-down “ $\Lambda$ ” pattern. This phenomenon has often been observed in some compounds with AIE properties, but the reasons remain unclear.<sup>13</sup> To better understand the luminescence behavior and mechanism of the compounds in solvent mixtures, we carried out the following study in detail.

As can be seen in Table 1, the fluorescence quantum yield ( $\Phi_F$ ) of compounds 1–6 with a water fraction of 30% are higher

Table 1 Fluorescence quantum yields (QY) obtained after water was injected for 24 hours<sup>a</sup>

QY	$f_w = 0\%$	$f_w = 30\%$	$f_w = 60\%$	$f_w = 90\%$
1	<0.1%	37.2%	17.8%	5.4%
2	<0.1%	26.6%	11.3%	1.8%
3	<0.1%	27.7%	7.9%	1.9%
4	<0.1%	28.0%	12.1%	<0.1%
5	<0.1%	25.4%	12.2%	1.9%
6	<0.1%	35.3%	14.3%	0.3%

<sup>a</sup>  $f_w$ : water fraction.

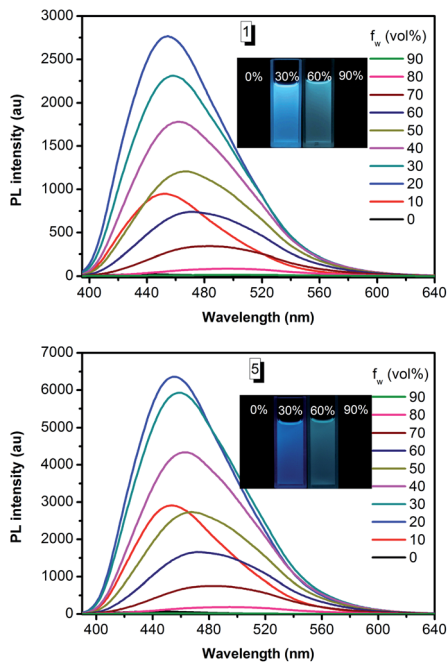


Fig. 5 PL spectra of the dilute solutions of **1** and **5** in water–THF mixtures with different volume fractions of water (excitation wavelength = 365 nm) after water was injected for 24 hours (10  $\mu$ M). The insets show the emission images of **1** and **5** in pure THF, as well as in solvent mixtures with 30%, 60% and 90% water contents taken under 365 nm UV illumination at room temperature (10  $\mu$ M), respectively.

than that with the water fractions of 60% and 90%. Hence, the addition of water may effectively influence the conformation of molecules to some extent. The similar quenched emission and low fluorescence efficiency (Table 1) of **1–6** in pure THF and mixtures with a high water contents (>80%) suggests that they may possess properties of AIEE.<sup>14</sup>

To further prove our hypothesis, we followed the time course of spectral evolution of **1–6** (**1**, **5** in Fig. 6, **2–4** and **6** in Fig. S5†) in mixtures with different water contents. Interestingly, the emission intensity of a prepared aqueous mixture changed constantly with time at room temperature. As depicted in Fig. 6, the PL spectra of compounds **1** and **5** show a remarkable enhancement in the emission intensity with low water fractions. In contrast, almost no changes in the PL spectra of the compounds are observed in the aqueous mixtures with over 80% water contents, even after the mixture has been allowed to stand for as long as 24 h. As the compounds have a good solubility in a low hydration mixture, there are hardly any nanoparticles available within a short time period. However, as time passes, the molecules may gradually self-assemble to crystal particles, giving a time-dependent fluorescence enhancement.<sup>15</sup> On the other hand, in the solvent mixture with 90% water content, the molecules may disperse to amorphous nanoparticles. From the absorption with no tailed peak of compounds **1–6** in a low water fraction in Fig. 4 and the obvious enhancement of emission in the mixture of low water fraction (<30%), one can find that despite there being no tailed peak in the mixture with a low water contents, the emission can still be

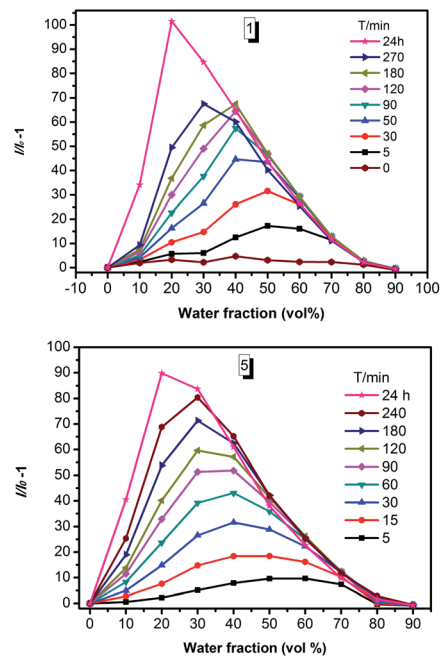


Fig. 6 Time-dependent changes of **1** and **5** in the PL peak intensity (10  $\mu$ M).

enhanced with time. The fluorescent intensity enhancement of **1–6** with 30% water fractions increased from 32, 17, 14, 2, 32, 0.4 times to 102, 35, 62, 10, 90, 9 times after water was added for 24 hours. Fig. 7 shows the photographs of a solution mixture taken under the UV illumination with 50% water contents. As the time goes from 0 min, to 30 min to 50 min, the fluorescence intensity shows an enhancement of 30 times and 45 times compared with that of 0 min, respectively.

### SEM and TEM observation

The scanning electron microscopy (SEM) images of **1**, **5** and **6** in the THF–water mixtures with low and high water contents at different times are shown in Fig. 8, which show the existence of aggregation in the solvent mixture. For **1** with 50% water contents (Fig. 8a), the particle size was about 200–300 nm. A globular particle of **1** with 70% water content after water was injected for 1 hour (Fig. 8b) can be observed in a form of fusion. After water was injected for 2.5 hours, the molecules grew into

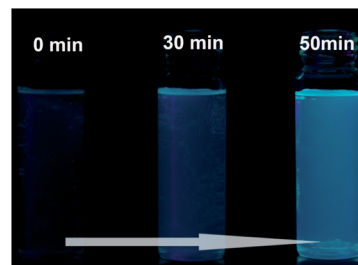


Fig. 7 Photographs of **1** in the THF/H<sub>2</sub>O mixtures with 50% water contents at different times taken under UV illumination (10  $\mu$ M).

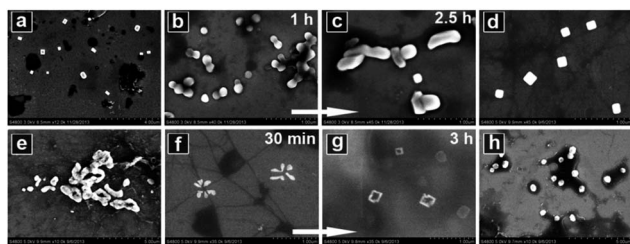


Fig. 8 SEM of **1** ((a) 50%, 3 h, (b) 70%, 1 h and (c) 70% 2.5 h), **5** ((d) 50%, 2 h and (e) 70%, 3 h) and **6** ((f) 30%, 30 min, (g) 30%, 3 h and (h) 90%, 30 min) formed in the THF–water mixtures containing different water contents in different time ranges after the water was injected.

larger rods with the shape of rounded strips, with widths of  $\sim 200$  nm and various lengths ranging from 200–600 nm. Similar to **1**, **5** has a square structure after water was injected for 2 hours with 50% water content (Fig. 8d), indicating some kind of specific arrangement of molecules. **5** shows irregular round strips (Fig. 8e) after water was injected for 3 h with 70% water content, which is similar to **1** (Fig. 8c). Particles of **6** with 30% water content change from an amorphous form (Fig. 8f) with a diameter of nearly 150 nm after water was injected for 30 min to a crystalline form (Fig. 8g) with a diameter of 300–400 nm after water was injected for 3 h. Initially only a small portion of the compound molecules probably cluster together to form tiny nanoparticles. The larger portion of the compound molecules remaining in the solvent mixture then gradually deposits onto the initially formed nanoparticles in a way similar to recrystallization. The aggregations of **6** with 90% water content after water was injected for 30 min (Fig. 8h) can be observed in the form of globes. Almost no change in the diameters and morphology can be observed, even after water was injected for 24 h in the solvent mixtures (Fig. S6<sup>†</sup>).

As shown in Fig. S7<sup>†</sup> aggregates with an average diameter of  $\sim 670$  nm formed in the aqueous mixture with 70% water content after water was injected for 30 min and grew up to  $\sim 1091$  nm after water was injected for 3 hours. In comparison to the size of the aggregates of **6** at 70% water contents, no obvious change in the diameters can be observed, despite the interval of 23.5 hours, which is in accordance with the initial speculation.

The transmission electron microscopy (TEM) images of **1** in the THF–water mixtures with different water contents (30%, 50%, 70% and 90%) are shown in Fig. 9. The insets of Fig. 9(a–d) show the electron diffraction (ED) patterns of the aggregates formed in the THF–water mixtures with 30%, 50%, 70% and 90% water contents, respectively. The dark regular structures in the photographs are the beam stop used to protect the detector from the intense main undiffracted beam. A series of clear diffraction spots surrounding the main undiffracted beam can be observed in Fig. 9a, indicating that the aggregates are crystalline or that the compound molecules are packed in an ordered fashion.<sup>16</sup> In the mixtures with low water fractions, molecules of **1** may cluster together slowly in an ordered fashion to form crystal-like aggregations. When the water fraction becomes high ( $>80\%$ ), its molecules may aggregate instantly to form globular particles with no diffraction spots (Fig. 9d). As the

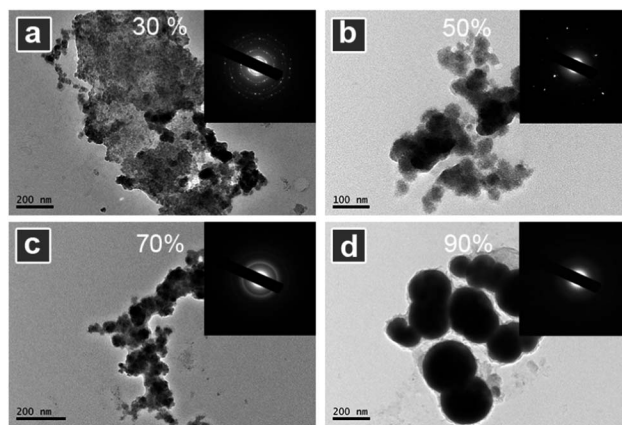


Fig. 9 TEM images and ED patterns of crystalline (a–c) and amorphous nanoaggregates of **1** formed in the THF–water mixtures containing 30% (a), 50% (b), 70% (c) and 90% (d) water contents after water was injected for 12 hours, 2 hours, 1 hour and 24 hours, respectively.

water contents changes from low to high, the quantity of diffraction spots changed from more to less. Since there is only a dim diffraction ring observed in Fig. 9d, the nanoparticles are thus amorphous in nature.

The different rate of fluorescence intensity enhancement of compounds **1–6** in their solvent mixtures with the different water contents (Fig. 6 and S5<sup>†</sup>) may be attributed to the different speeds of crystallization related to their different solvent environments.<sup>17</sup> As shown in Fig. S8<sup>†</sup>, only two diffraction spots can be observed after water was injected for 40 min, however, many of them appeared (Fig. S8b) after 1 hour and 20 minute, which may account for the time-dependent enhancement of fluorescence emission.

#### Different properties in different states

To gain further insight into the CEE properties of compounds **1–6**, we obtained a series of PL measurements in powder, film, the pure solution and mixed solutions with  $f_w = 30\%$  (Fig. 10 and S9<sup>†</sup>). As we can see from Table 2, compound **1** shows the value of  $\lambda_{em}$  as being in the order of the pure solution  $<$  the solution mixture ( $f_w = 30\%$ )  $<$  film  $<$  powder. The same order can also be observed in **2–4**, **6**. (a) In the powder state, the molecules adopted the arrangement of having relatively good planarity, which offers the molecules relatively strong charge delocalization. (b) In the pure solution, the compounds are molecularly isolated without any interactions between the adjacent molecules. Hence, molecules may distort without the intermolecular restriction, giving an emission of blue-shift. (c) The molecules in the film state have an emission wavelength similar to that in the powder state, which is quite different from the wavelength in the pure solution. It is probably because the concentration of the solution may increase as the solvent gradually evaporates, and majority of the isolated molecules agglomerate again.<sup>18</sup> (d) The curves of the solution mixture show a middle location in contrast to the other three states, which indicated that some weak forces may be formed after water was injected to restrict the rotation of the aromatic

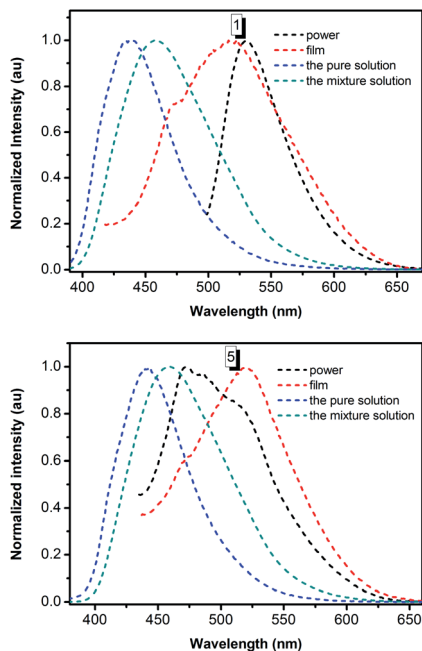


Fig. 10 Photoluminescence spectra of **1** and **5** in powder, film, pure THF solution and the solvent mixture with 30% water contents (10  $\mu$ M) after the water was injected for 24 h.

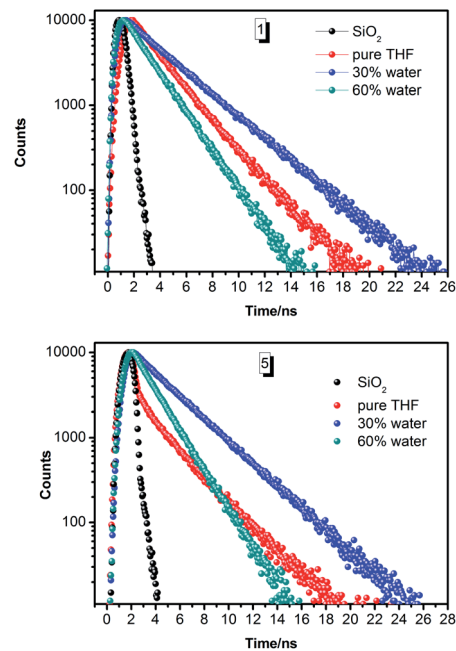


Fig. 11 PL lifetime spectra of **1** and **5** in pure solution, solution mixtures with 30% water content and 60% water content (10  $\mu$ M).

Table 2 Maximum emission wavelength of **1**–**6** in different states<sup>a</sup>

	$\lambda_{em}/nm$					
	<b>1</b>	<b>2</b>	<b>3</b>	<b>4</b>	<b>5</b>	<b>6</b>
Powder	531	—	537	523	472	548
Film	516	—	531	513	520	544
THF	437	436	442	437	443	438
Mixtures	458	458	459	459	460	458

<sup>a</sup> No signal of emission in powder and film was obtained for **2**.

rings,<sup>19</sup> giving a red-shift emission in contrast to the location in the pure solution. As to the abnormal blue-shift of **5** in the powder state, the reason may be that its molecules have relatively larger aromatic rings, which enforces distortion of the molecules to a large extent to avoid complanation.<sup>20</sup>

The time-resolved fluorescence measurements of **1** and **5** are shown in Fig. 11 (others in Fig. S10<sup>†</sup>), and the detailed data of the fluorescence decay curves of **1**–**6** are listed in Table S3.<sup>†</sup> The experimental errors are estimated to be  $\pm 13\%$  from the sample concentrations and instruments. The lifetimes of **1**–**6** in different water fractions are obtained by monitoring at the monomer emission. The decay behavior of **1**–**6** is in a double-exponential manner in the solution mixture obtained by monitoring at the monomer emission. The lifetimes of **1**–**6** with the water fraction of 0% is contributed to by the two lifetime species, while the lifetime of **1**–**6** in the water fractions of 30% and 60% is almost entirely from the contribution of the longer lifetime species. As shown in Table S3,<sup>†</sup> the weighted mean lifetime of **1** in 30% water fraction (3.15 ns) is longer than that of **1** in 0% and 60% water fractions (2.14 ns

and 1.73 ns, respectively). The same tendency can also be found in the other five compounds, which implies that the formation of crystalline aggregates restricts the rotation and vibration of the groups in the molecules, so that longer emission lifetimes were detected.<sup>21</sup> The relatively low water contents may make the molecules more conducive to self-organization. The lowest lifetimes were observed at 60% water content, which may be due to the combined action of the increasing solvent polarity and the amorphous aggregation.<sup>22</sup>

## Conclusions

In summary, we have designed and synthesized six molecules (**1**–**6**) with different terminal aromatic rings. All the compounds are almost non-emissive when dissolved in pure THF, but become strongly emissive when aggregated in aqueous solvents. Efficient emission enhancement can be achieved with relatively low water contents ( $\leq 60\%$ ) solutions containing crystalline phase, while low or even no emission is realized in the amorphous phase formed in solutions with high water contents ( $>60\%$ ). When the water ratio reaches 20% (**1** and **5**) or 30% (**2**–**4**, **6**) after water was injected for 24 hours, the PL intensity reached its maximum value. All compounds in the solvent mixtures with 30% and 60% water contents exhibit enhanced blue and cyan fluorescence emissions with time-dependence, respectively. The decreasing diffraction spots in aqueous mixtures with the increasing water contents suggests that compounds **1**–**6** are CEE-active materials. Evidently, a simple manipulation of the composition mixture or a small variation in the assembling environment may lead to the big change in the emission efficiency of **1**–**6**.

## Experimental

### General information

All chemicals were available commercially. All the chemicals were used directly without further purification. THF was HPLC grade from BODI Organic Company and was used as received.

### Instruments

The NMR spectra were recorded on a 400 MHz NMR instrument. Chemical shifts were reported in parts per million (ppm) relative to internal TMS (0 ppm) and coupling constants in hertz. Splitting patterns were described as singlet (s), doublet (d), triplet (t) or multiplet (m). The IR spectra were recorded with a Nicolet FT-IR NEXUS 870 spectrometer (KBr discs). The UV-vis absorption spectra were recorded on a UV-3100 spectrophotometer. The mass spectra were obtained on an autoflex speed MALDI-TOF/TOF mass spectrometer. The scan electron microscopy (SEM) and transmission electron microscopy (TEM) studies were performed using a Hitachi S-4800 scanning electron microscope and JEOL JEM-100SX transmission electron microscope. Dynamic light scattering (DLS) measurements were conducted on a Malvern Zeta Nano-ZS90 Particle Size Analyzer. Fluorescence measurements were carried out using an Edinburgh FLS920 fluorescence spectrometer equipped with a 450 W Xe lamp and a time-correlated single-photon counting (TCSPC) card. For the time-resolved fluorescence measurements, the fluorescence signals were collimated and focused onto the entrance slit of a monochromator with the output plane equipped with a photomultiplier tube. The absolute photoluminescence quantum yield ( $\Phi_F$ ) values of the mixture with different water fractions (0%, 30%, 60%, 90%;  $1 \times 10^{-5}$  M) were determined using an integrating sphere.

### Preparation and characterization

**Synthesis of a.** Sodium hydroxide (24.0 g, 0.6 mol) and 4-iodo-phenol (120.0 g, 0.54 mol) were crushed together in batches with a pestle and mortar. Then bromoethane (300 mL) was added to this white powder. To this solution, cesium hydroxide (10 g) in 20 mL of DMF and 3 drops of 18-crown-6 were added and stirred for 1 h at room temperature. Then the reaction mixture was heated at 60 °C for 78 h. The mixture was concentrated and cooled to room temperature (RT) after the reaction was completed by monitoring with thin-layer chromatography (TLC). Much water was added and the mixture was extracted with dichloromethane (100 mL) three times. The organic extracts were dried over  $\text{MgSO}_4$ . After removing the solvents under reduced pressure, a red oily liquid was obtained (128.4 g, yield: 94.9%).

**Synthesis of b.** Aniline (5.0 g, 54 mmol) and 1-ethoxy-4-iodobenzene (46.0 g, 185 mmol) were added to 1,2-dichlorobenzene (200 mL) in a three-neck flask. Potash (17.94 g, 130 mmol) and copper powder (8.34 g, 130 mmol) were slowly added to the mixture after stirring for a short moment in an atmosphere of nitrogen. Three drops of 18-crown-6 were added to the mixture. The mixture was reacted at 180 °C for 12 h. After the reaction was completed, it was cooled to RT. The solvents were removed

under reduced pressure and the mixture was purified by chromatography on silica gel using petroleum ether/ethyl acetate (50 : 1, v/v) as the eluent, giving white crystals **b**, 7.8 g, yield: 43.6%.  $^1\text{H-NMR}$  (400 MHz,  $(\text{CD}_3)_2\text{CO}$ ),  $\delta$  (ppm): 7.18–7.14 (t,  $J = 7.6$  Hz, 2H), 7.02–7.00 (d,  $J = 8.4$  Hz, 4H), 6.86–6.71 (m, 7H), 4.04–3.99 (m, 4H), 1.37–1.34 (t,  $J = 7.0$  Hz, 6H).

**Synthesis of c.**  $\text{POCl}_3$  (2.3 mL) was added dropwise to freshly distilled DMF (2.8 mL) which was stirred in a flask (150 mL) with ice water bath cooling. After 30 min, the solution become sticky and was stirred a little longer to yield a reddish salt resembling ice. Then the salt was combined with a portion of **b** (5.0 g, dissolved in 15 mL chloroform) to yield a reddish solution. Then the reaction mixture was heated at 65 °C for 10 h. The reaction was monitored by TLC. After the reaction was completed, it was concentrated. The black mixture was dissolved in dichloromethane and then poured into a large amount of water.  $\text{Na}_2\text{CO}_3$  solution (40%) was added to adjust the pH of the mixture to 7–8. The mixture was extracted three times with dichloromethane and the organic extracts were dried over  $\text{MgSO}_4$ . After removing solvents under reduced pressure, the mixture was purified by chromatography on silica gel using petroleum ether/ethyl acetate (40 : 1, v/v) as the eluent, giving a yellow oily product 5.21 g, yield: 96.15%.  $^1\text{H-NMR}$  (400 MHz,  $(\text{CD}_3)_2\text{CO}$ ),  $\delta$  (ppm): 9.76 (s, 1H), 7.67–7.65 (d,  $J = 8.4$  Hz, 2H), 7.19–7.17 (d,  $J = 8.8$  Hz, 4H), 6.98–6.96 (d,  $J = 8.4$  Hz, 4H), 6.78–6.76 (d,  $J = 8.8$  Hz, 2H), 4.07–4.02 (m, 4H), 1.38–1.35 (t,  $J = 7.0$  Hz, 6H).

**Synthesis of d.** A DMF solution containing 4-nitro-benzene-1,2-diamine (1.3 g, 8.3 mmol) and KI (0.55 g) was added to a DMF solution containing 4-[bis-(4-ethoxyphenyl)-amino]-benzaldehyde (3 g, 8.3 mmol). The mixture was then refluxed by stirring for 16 h. After the reaction was completed, the reaction mixture was cooled to room temperature and poured into water to yield a large amount of precipitate. Then the precipitate was filtrated and washed with water three times. The crude product was purified by chromatography on silica gel using petroleum ether/ethyl acetate (5 : 1, v/v) as the eluent, giving a red powdered solid 2.9 g, yield: 71%.  $^1\text{H-NMR}$  (400 MHz,  $\text{DMSO}-d_6$ ),  $\delta$  (ppm): 13.30 (s, 1H), 8.45–8.28 (d,  $J = 7.2$  Hz, 1H), 8.11–8.06 (t,  $J = 8.6$  Hz, 1H), 8.00–7.98 (m, 2H), 7.75–7.62 (m, 1H), 7.15–7.13 (d,  $J = 8.4$  Hz, 4H), 6.97–6.95 (d,  $J = 8.8$  Hz, 4H), 6.82–6.80 (d,  $J = 8.8$  Hz, 2H), 4.05–4.00 (m, 4H), 1.35–1.32 (t,  $J = 6.8$  Hz, 6H); MS (MALDI-TOF):  $m/z$  493.575  $[(M - 1)^+]$ , calcd 493.195.

**Synthesis of e.** Hydrazine hydrate (19 mL) was added dropwise to ethanol (50 mL) containing bis-(4-ethoxyphenyl)-[4-(5-nitro-1H-benzoimidazol-2-yl)-phenyl]-amine (1.9 g, 3.84 mmol). Then the mixture was refluxed by stirring for 20 min and 0.15 g  $\text{Pd}(\text{OAc})_2$  was added to the mixture. After stirring for one more hour, the solution started to become a yellow transparent solution. The reaction mixture was then cooled to room temperature and concentrated. A yellow solid was obtained (1.456 g, 3.14 mmol), yield: 81.6%.  $^1\text{H-NMR}$  (400 MHz,  $\text{DMSO}-d_6$ ),  $\delta$  (ppm): 12.01 (s, 1H), 7.86–7.84 (d,  $J = 8.4$  Hz, 2H), 7.23–7.22 (d,  $J = 7.6$  Hz, 1H), 7.08–7.06 (d,  $J = 8.4$  Hz, 4H), 6.93–6.91 (d,  $J = 8.8$  Hz, 4H), 6.80–6.78 (d,  $J = 8.8$  Hz, 2H), 6.62 (s, 1H), 6.49–6.47 (d,  $J = 7.6$  Hz, 1H), 4.87 (s, 2H), 4.03–3.98 (m, 4H), 1.34–1.31 (t,  $J = 6.8$  Hz, 6H); MS (MALDI-TOF):  $m/z$  463.936  $[(M - 1)^+]$ , calcd 463.221.

**Synthesis of compounds 1–3.** Compound 1: 0.3 g (0.43 mmol) 2-{4-[bis-(4-ethoxyphenyl)-amino]-phenyl}-1*H*-benzoimidazol-5-ylamine was added to a benzene solution (10 mL) and the mixture was stirred at 35 °C for a moment. Then a mixed solution of 0.046 g (0.43 mmol) pyridine-2-carbaldehyde and two drops of glacial acetic acid were added to the mixture and the solid was dissolved quickly. The mixture was reacted for 15 h and then cooled to room temperature. A faint yellow powder was obtained through vacuum filtration (0.15 g), yield: 63.1%. <sup>1</sup>H-NMR (400 MHz, DMSO-*D*<sub>6</sub>),  $\delta$  (ppm): 12.80 (s, 1H), 8.73 (s, 2H), 8.22–8.20 (d,  $J = 8.0$  Hz, 1H), 8.01–7.99 (d,  $J = 8.4$  Hz, 2H), 7.97–7.93 (t,  $J = 7.6$  Hz, 1H), 7.65–7.63 (d,  $J = 8.4$  Hz, 1H), 7.53–7.48 (m, 2H), 7.29–7.28 (d,  $J = 6.8$  Hz, 1H), 7.11–7.09 (d,  $J = 8.4$  Hz, 4H), 6.94–6.92 (d,  $J = 8.4$  Hz, 4H), 6.84–6.82 (d,  $J = 8.4$  Hz, 2H), 4.02–3.97 (m, 4H), 1.34–1.30 (t,  $J = 6.8$  Hz, 6H); <sup>13</sup>C-NMR (100 MHz, DMSO-*D*<sub>6</sub>),  $\delta$  (ppm): 159.06, 156.25, 155.01, 153.36, 160.57, 150.18, 145.41, 139.64, 137.53, 128.17, 125.84, 121.53, 121.13, 118.06, 116.08, 63.75, 15.28; IR (KBr, cm<sup>-1</sup>): 3379, 3150, 2976, 1611, 1546, 1506, 1472, 1447, 1393, 1284, 1241, 1194, 1167, 1115, 1048, 961, 923, 830; MS (MALDI-TOF):  $m/z$  552.760 [(*M* - 1)<sup>+</sup>, calcd 552.248]. Compound 2: The synthesis of 2 was similar to that of 1. Yield: 84.1%. <sup>1</sup>H-NMR (400 MHz, DMSO-*D*<sub>6</sub>),  $\delta$  (ppm): 12.76 (s, 1H), 9.10 (s, 1H), 8.82 (s, 1H), 8.70–8.69 (d,  $J = 4.4$  Hz, 1H), 8.35–8.33 (d,  $J = 7.6$  Hz, 1-H, d-H), 8.00–7.98 (d,  $J = 8.0$  Hz, 2H), 7.62 (s, 1H), 7.56–7.43 (m, 2H), 7.25–7.24 (d,  $J = 6.8$  Hz, 1H), 7.11–7.09 (d,  $J = 8.4$  Hz, 4H), 6.94–6.92 (d,  $J = 8.4$  Hz, 4H), 6.84–6.81 (d,  $J = 8.4$  Hz, 2H), 4.02–3.97 (m, 4H), 1.34–1.31 (t,  $J = 6.8$  Hz, 6H); <sup>13</sup>C-NMR (100 MHz, DMSO-*D*<sub>6</sub>),  $\delta$  (ppm): 156.93, 156.24, 153.15, 152.11, 150.87, 150.53, 146.14, 139.66, 135.29, 132.48, 128.14, 124.60, 121.19, 118.11, 116.09, 63.76, 15.28; IR (KBr, cm<sup>-1</sup>): 3396, 3165, 2976, 1607, 1546, 1505, 1474, 1448, 1393, 1288, 1240, 1193, 1167, 1115, 1048, 962, 923, 828; MS (MALDI-TOF):  $m/z$  552.248 [(*M* - 1)<sup>+</sup>, calcd 552.346]. Compound 3: The synthesis of 3 was also similar to that of 1. Yield: 63.1%. <sup>1</sup>H-NMR (400 MHz, DMSO-*D*<sub>6</sub>),  $\delta$  (ppm): 12.76 (s, 1H), 8.80 (s, 1H), 8.75–8.74 (s,  $J = 4.8$  Hz, 2H), 7.98–7.96 (d,  $J = 8.4$  Hz, 2H), 7.88–7.87 (d,  $J = 4.4$  Hz, 2H), 7.63–7.62 (d,  $J = 6.8$  Hz, 1H), 7.51–7.45 (m, 1H), 7.28–7.26 (d,  $J = 7.6$  Hz, 1H), 7.13–7.11 (d,  $J = 8.4$  Hz, 4H), 6.96–6.94 (d,  $J = 8.4$  Hz, 4H), 6.83–6.80 (d,  $J = 8.4$  Hz, 2H), 4.05–4.00 (m, 4H), 1.35–1.32 (t,  $J = 6.8$  Hz, 6H); <sup>13</sup>C-NMR (100 MHz, DMSO-*D*<sub>6</sub>),  $\delta$  (ppm): 157.23, 156.25, 153.47, 150.95, 150.60, 145.44, 143.46, 139.63, 128.15, 122.64, 121.09, 118.09, 116.07, 63.75, 15.26; IR (KBr, cm<sup>-1</sup>): 3414, 3145, 2977, 1602, 1550, 1504, 1476, 1448, 1394, 1286, 1239, 1192, 1167, 1115, 1045, 960, 922, 823; MS (MALDI-TOF):  $m/z$  552.248 [(*M* - 1)<sup>+</sup>, calcd 552.030].

**Synthesis of compounds 4–6.** Compound 4: 0.3 g (0.43 mmol) 2-{4-[bis-(4-ethoxyphenyl)-amino]-phenyl}-1*H*-benzoimidazol-5-ylamine was added to a methanol solution (10 mL) and the mixture was stirred at 35 °C for a moment. Then a mixed solution of 0.046 g (0.43 mmol) benzaldehyde and one drop of glacial acetic acid was added to the mixture and the solid was dissolved quickly. The reaction was monitored by TLC. Not until 9 hours afterwards had the mixture completely reacted. Then the solvent was removed under vacuum. DMF (5 mL) was put into the product. The mixture was put into water (80 mL) after the product was fully dissolved. A yellowish white powder was

obtained through vacuum filtration (0.32 g), yield: 84%. <sup>1</sup>H-NMR (400 MHz, DMSO-*D*<sub>6</sub>),  $\delta$  (ppm): 12.69(s, 1H), 8.72(s, 1H), 7.95–7.97 (d,  $J = 8.0$  Hz, 4H), 7.61–7.35 (m, 5H), 7.21–7.17 (t,  $J = 8.2$  Hz, 1H), 7.13–7.10 (d,  $J = 8.8$  Hz, 4H), 6.96–6.94 (d,  $J = 8.8$  Hz, 4H), 6.83–6.80 (d,  $J = 8.8$  Hz, 2H), 4.05–4.00 (m, 4H), 1.35–1.32 (t,  $J = 6.8$  Hz, 6H); <sup>13</sup>C-NMR (100 MHz, DMSO-*D*<sub>6</sub>),  $\delta$  (ppm): 158.66, 155.63, 152.38, 150.38, 149.88, 145.87, 139.09, 136.35, 134.24, 133.03, 131.65, 128.75, 128.45, 127.52, 122.71, 120.69, 119.24, 117.55, 115.5, 63.17, 14.68; IR (KBr, cm<sup>-1</sup>): 3408, 2980, 1607, 1505, 1473, 1449, 1390, 1288, 1238, 1193, 1166, 1112, 1046, 962, 921, 830; MS (MALDI-TOF):  $m/z$  553.396 [(*M* + 1)<sup>+</sup>, calcd 553.253]. Compound 5: 0.5 g (0.72 mmol) 2-{4-[bis-(4-ethoxyphenyl)-amino]-phenyl}-1*H*-benzoimidazol-5-ylamine was added to methanol solution (10 mL) and the mixture was stirred at 35 °C for a moment. Then a mixed solution of 0.112 g (0.72 mmol) 2-naphthaldehyde and one drop of glacial acetic acid was added to the mixture and the solid was dissolved quickly. The reaction was monitored through TLC. Not until 4 hours afterwards had the mixture completely reacted. A yellowish white powder was obtained through vacuum filtration (0.55 g), yield: 84.8%. <sup>1</sup>H-NMR (400 MHz, DMSO-*D*<sub>6</sub>),  $\delta$  (ppm): 12.722 (s, 1H), 8.889 (s, 1H), 8.41 (s, 1H), 8.20–8.18 (d,  $J = 8.4$  Hz, 1H), 8.05–7.97 (m, 5H), 7.61–7.43 (m, 4H), 7.27–7.25 (d,  $J = 8.0$  Hz, 1H), 7.13–7.11 (d,  $J = 8.8$  Hz, 4H), 6.96–6.94 (d,  $J = 8.8$  Hz, 4H), 6.83–6.81 (d,  $J = 8.8$  Hz, 2H), 4.04–4.01 (m, 4H), 1.35–1.32 (t,  $J = 6.8$  Hz, 6H); <sup>13</sup>C-NMR (100 MHz, DMSO-*D*<sub>6</sub>), 155.63, 152.43, 149.89, 139.09, 134.1, 132.74, 128.64, 128.40, 127.82, 127.53, 126.77, 123.58, 121.51, 120.68, 117.54, 115.51, 63.16, 14.68; IR (KBr, cm<sup>-1</sup>): 2973, 1609, 1547, 1503, 1475, 1445, 1390, 1284, 1238, 1195, 1167, 1117, 1046, 962, 924, 827; MS (MALDI-TOF):  $m/z$  603.417 [(*M* + 1)<sup>+</sup>, calcd 603.268]. Compound 6: the synthesis of compound 6 was almost the same as 5. Yield: 98%. <sup>1</sup>H-NMR (400 MHz, DMSO-*D*<sub>6</sub>),  $\delta$  (ppm): 13.50–13.43 (d,  $J = 27.6$  Hz, 1H), 12.77–12.76 (d,  $J = 5.2$  Hz, 1H), 9.04–9.03 (d,  $J = 3.2$  Hz, 1H), 7.98–7.96 (d,  $J = 8.4$  Hz, 2H), 7.70–7.63 (m, 2H), 7.52–7.49 (t,  $J = 7.2$  Hz, 1H), 7.42–7.38 (t,  $J = 8$  Hz, 1H), 7.31–7.28 (d,  $J = 8.4$  Hz, 1H), 7.13–7.10 (d,  $J = 8.4$  Hz, 4H), 7.00–6.94 (m, 6H), 6.83–6.81 (d,  $J = 8.8$  Hz, 2H), 4.05–3.99 (m, 4H), 1.35–1.32 (t,  $J = 6.8$  Hz, 6H); <sup>13</sup>C-NMR (100 MHz, DMSO-*D*<sub>6</sub>): 160.2, 155.65, 152.82, 150.00, 144.71, 139.04, 134.44, 132.39, 130.72, 127.55, 122.26, 120.45, 119.45, 119.00, 117.49, 116.48, 115.51, 63.17, 14.67; IR (KBr, cm<sup>-1</sup>): 2974, 1609, 1571, 1503, 1449, 1392, 1280, 1239, 1194, 1166, 1145, 1112, 1047, 963, 920, 827; MS (MALDI-TOF):  $m/z$  569.416 [(*M* + 1)<sup>+</sup>, calcd 569.247].

## Acknowledgements

This work was supported by the Program for New Century Excellent Talents in University (China), the Doctoral Program Foundation of the Ministry of Education of China (20113401110004), the National Natural Science Foundation of China (21271003, 21271004 and 51372003), the Natural Science Foundation of Education Committee of Anhui Province (KJ2012A024), the 211 Project of Anhui University, Higher Education Revitalization Plan Talent Project of (2013) and the Ministry of Education Funded Projects Focus on Returned Overseas Scholar.

## Notes and references

- 1 (a) K. T. Kamtekar, A. P. Monkman and M. R. Bryce, *Adv. Mater.*, 2010, **22**, 572–582; (b) S. J. Park, S. G. Kuang, M. Fryd, J. G. Saven and S. J. Park, *J. Am. Chem. Soc.*, 2010, **132**, 9931–9933.
- 2 (a) R. Jakubiak, C. J. Collison, W. Wan, L. J. Rothberg and B. R. Hsieh, *J. Phys. Chem. A*, 1999, **103**, 2394–2398; (b) S. W. Thomas, G. D. Joly and T. M. Swager, *Chem. Rev.*, 2007, **107**, 1339–1386.
- 3 J. D. Luo, Z. L. Xie, J. W. Y. Lam, L. Cheng, H. Y. Chen, C. F. Qiu, H. S. Kwok and B. Z. Tang, *Chem. Commun.*, 2001, 1740–1741.
- 4 B. K. An, S. K. Kwon, S. D. Jung and S. Y. Park, *J. Am. Chem. Soc.*, 2002, **124**, 14410–14415.
- 5 (a) L. J. Qian, B. Tong, J. B. Shen, J. B. Shi, J. G. Zhi and B. Z. Tang, *J. Phys. Chem. B*, 2009, **113**, 9098–9103; (b) W. Z. Yuan, X. Y. Shen, H. Zhao, J. W. Y. Lam, L. Tang and B. Z. Tang, *J. Phys. Chem. C*, 2010, **114**, 6090–6099; (c) C. M. Yang, I. W. Lee, T. L. Chen and J. L. Hong, *J. Mater. Chem. C*, 2013, **1**, 2842–2850.
- 6 (a) J. W. Chen, B. Xu, B. Z. Tang and Y. Cao, *J. Phys. Chem. A*, 2004, **108**, 7522–7526; (b) K. Itami, Y. Ohashi and J. i. Yoshida, *J. Org. Chem.*, 2005, **70**, 2778–2792.
- 7 (a) W. Huang, H. T. Zhou, B. Li and J. H. Su, *RSC Adv.*, 2013, **3**, 3038; (b) M. Liang, W. Xu, F. S. Cai and Z. M. Li, *J. Phys. Chem. C*, 2007, **111**, 4465–4472; (c) H. M. Tian, X. C. Yang, R. K. Chen and L. C. Sun, *J. Phys. Chem. C*, 2008, **112**, 11023–11033.
- 8 F. Sączewska, P. J. Bednarski and R. Grünertb, *J. Inorg. Biochem.*, 2006, **100**, 1389–1398.
- 9 L. K. Wang, Z. Zheng, Z. P. Yu, J. Zheng, J. Y. Wu, Y. P. Tian and H. P. Zhou, *J. Mater. Chem. C*, 2013, **1**, 6952–6959.
- 10 C. W. Chang, C. J. Bhongale, C. S. Lee, W. K. Huang, C. S. Hsu and E. W. G. Diau, *J. Phys. Chem. C*, 2012, **116**, 15146–15154.
- 11 W. Z. Yuan, Y. Y. Gong, S. M. Chen, X. Y. Shen and B. Z. Tang, *Chem. Mater.*, 2012, **24**, 1518–1528.
- 12 (a) Q. Q. Li, J. H. Zou, J. W. Chen, Z. J. Liu and Y. Cao, *J. Phys. Chem. B*, 2009, **113**, 5816–5822; (b) J. Liu, Q. Meng, X. T. Zhang, X. Q. Lu, P. He and W. P. Hu, *Chem. Commun.*, 2013, **49**, 1199–1206.
- 13 (a) Y. Q. Dong, J. W. Y. Lam, A. J. Qin, Z. Li and B. Z. Tang, *Chem. Commun.*, 2007, 3255–3257; (b) H. Tong, Y. Q. Dong, J. W. Y. Lam and B. Z. Tang, *Chem. Commun.*, 2006, 1133–1135.
- 14 T. Y. Han, Y. N. Hong, N. Xie, S. J. Chen, N. Zhao, E. G. Zhao, J. W. Y. Lam, H. M. H. Y. Sung, Y. P. Dong, B. Tong and B. Z. Tang, *J. Mater. Chem. C*, 2013, **1**, 7314–7320.
- 15 Y. Qian, S. Y. Li, G. Q. Zhang, Q. Wang, S. Q. Wang, H. J. Xu and G. Q. Yang, *J. Phys. Chem. B*, 2007, **111**, 5861–5868.
- 16 T. Tong, Y. N. Hong, Y. Q. Dong and B. Z. Tang, *J. Phys. Chem. B*, 2007, **111**, 2000–2007.
- 17 J. Wang, J. Mei, R. R. Hu, J. Z. Sun, A. J. Qin and B. Z. Tang, *J. Am. Chem. Soc.*, 2012, **134**, 9956–9966.
- 18 Z. P. Yu, Y. Y. Duan, L. H. Cheng, Z. L. Han, H. P. Zhou, J. Y. Wu and Y. P. Tian, *J. Mater. Chem.*, 2012, **22**, 16927–16932.
- 19 M. D. Yang, D. L. Xu, W. G. Xi, L. K. Wang, H. P. Zhou, J. Y. Wu and Y. P. Tian, *J. Org. Chem.*, 2013, **78**, 10344–10359.
- 20 Z. Zheng, Z. P. Yu, M. D. Yang, F. Jin, Q. Zhang, H. P. Zhou, J. Y. Wu and Y. P. Tian, *J. Org. Chem.*, 2013, **78**, 3222–3234.
- 21 C. Y. Bao, R. Lu, M. Jin, P. C. Xue and Y. Y. Zhao, *Org. Biomol. Chem.*, 2005, **3**, 2508–2512.
- 22 X. Q. Zhang, Z. G. Chi, H. Y. Li, B. J. Xu and J. R. Xu, *J. Mater. Chem.*, 2011, **21**, 1788–1796.